3D Reconstruction of Coronary Arteries from Monoplane Angiography

Muhammad Abdul Rafey Farooqi[1] MFAROOQI.BESE21SEECS@SEECS.EDU.PK
Muhammad Zakwaan[1] MZAKWAAN.BEE22SEECS@SEECS.EDU.PK
Muhammad Saad Farhan[1] MMALIK.BEE21SEECS@SEECS.EDU.PK
Muhammad Jameel Nawaz[1] MUHAMMAD.JAMEEL@SEECS.EDU.PK
[1] *School of Electrical Engineering and Computer Science (SEECS), NUST, Islamabad*

Abstract

Invasive Coronary Angiography (ICA) remains the gold standard for diagnosing Coronary Artery Disease (CAD); however, its reliance on two-dimensional projections introduces significant limitations, including vessel foreshortening and overlap. This paper presents an automated computer vision pipeline for the three-dimensional reconstruction of coronary arteries from standard, non-simultaneous monoplane angiographic sequences. Utilizing the anonymized CADICA dataset, we address critical challenges inherent to retrospective clinical data, specifically the absence of geometric acquisition metadata and asynchronous video recording. Our methodology integrates Contrast Limited Adaptive Histogram Equalization (CLAHE) for image enhancement, Frangi filtering for robust vessel skeletonization, and a heuristic temporal synchronization logic to align cardiac phases across views. To resolve the unknown epipolar geometry, we implemented a blind geometric optimization algorithm that estimates camera pose via grid search minimization of the Reprojection Root Mean Square Error (RMSE). Experimental results demonstrate that the pipeline successfully recovers the 3D topology of the Left Anterior Descending (LAD) artery with a mean RMSE of approximately 35 pixels. While geometric drift was observed in distal segments due to uncalibrated acquisition parameters, the system achieved high morphological fidelity in proximal segments (< 10 pixels error). This work validates the feasibility of 3D morphological assessment from incomplete monoplane data, providing a foundation for low-cost, retrospective virtual surgical planning.

Keywords: 3D Reconstruction, Coronary Angiography, Computer Vision, Epipolar Geometry, Medical Imaging.

1. Introduction

Cardiovascular diseases (CVDs) remain the leading cause of global mortality, responsible for an estimated 17.9 million deaths annually (World Health Organization, 2021). Among these, Coronary Artery Disease (CAD) is the most prevalent manifestation, characterized by the narrowing or blockage of coronary arteries due to atherosclerotic plaque buildup. Accurate assessment of the severity and geometric configuration of these stenoses is critical for determining appropriate revascularization strategies, such as Percutaneous Coronary Intervention (PCI) or Coronary Artery Bypass Grafting (CABG).

Currently, Invasive Coronary Angiography (ICA) is considered the gold standard for diagnosing CAD (Scanlon et al., 1999). In standard clinical practice, physicians rely on

visual assessment of 2D X-ray projections to estimate the percentage of vessel narrowing. While Quantitative Coronary Angiography (QCA) tools have improved the reproducibility of these measurements (Reiber et al., 1985), inherent limitations persist. A fundamental drawback of 2D angiography is the loss of depth information, leading to vessel foreshortening and overlap. Studies have shown that 2D projections can result in significant errors in lesion length estimation and bifurcation angle assessment, potentially influencing clinical decision-making (Tuy, 2000).

To address these limitations, three-dimensional (3D) reconstruction of coronary arteries has emerged as a powerful diagnostic tool. 3D modeling eliminates foreshortening artifacts, provides accurate vessel topology, and enables advanced functional assessments such as Fractional Flow Reserve (FFR) simulation directly from angiographic data (Tu et al., 2014). Typically, 3D reconstruction is performed using biplane angiography systems, which acquire two simultaneous orthogonal views (Chen and Carroll, 2000). However, many catheterization laboratories rely on monoplane systems, where views are acquired sequentially rather than simultaneously.

Reconstructing 3D geometry from monoplane sequences presents significant computational challenges, primarily due to the asynchronous nature of the recordings. The cardiac phase, respiratory motion, and contrast agent dynamics differ between the two sequential acquisitions (Metz et al., 2009). Furthermore, retrospective analysis of anonymized medical datasets often introduces the "blind geometry" problem, where critical DICOM metadata describing the C-arm acquisition angles is absent.

In this paper, we present an automated computer vision pipeline for the 3D reconstruction of coronary arteries from monoplane angiographic videos. Utilizing the CADICA dataset (Jiménez-Partinen et al., 2024), we address the challenges of missing geometric metadata and temporal misalignment. We propose a robust methodology integrating contrast enhancement, vessel skeletonization, and a blind geometric optimization algorithm to recover 3D vessel topology without explicit camera calibration parameters.

2. Methodology

The proposed 3D reconstruction pipeline is composed of five sequential modules: (1) Image Preprocessing, (2) Vessel Segmentation and Skeletonization, (3) Temporal Synchronization, (4) Geometric Optimization, and (5) Surface Modeling. The workflow is designed to operate on raw monoplane angiographic videos without manual intervention.

2.1. Image Preprocessing

Raw angiographic images often suffer from non-uniform illumination and low contrast, where vessel structures are obscured by the spinal column and diaphragm. To mitigate this, we applied Contrast Limited Adaptive Histogram Equalization (CLAHE) (Pizer et al., 1987). Unlike global histogram equalization, CLAHE operates on small localized regions (tiles), enhancing local contrast while limiting noise amplification. For this study, we utilized a tile grid size of 8×8 and a clip limit of 2.0, effectively normalizing the intensity distribution across the vessel tree.

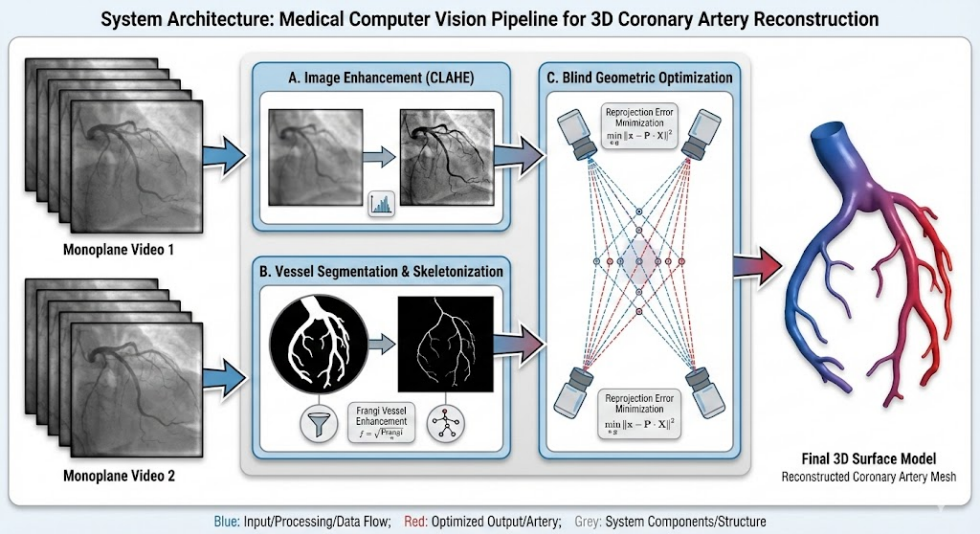

Figure 1: System architecture for 3D reconstruction from uncalibrated monoplane data. The pipeline addresses the absence of geometric metadata by integrating heuristic temporal synchronization with a blind geometric optimization algorithm that estimates camera pose by minimizing Reprojection RMSE. The final output is a B-Spline interpolated generalized cylinder model.

2.2. Vessel Segmentation and Tracking

To extract the vessel topology, we employed a Hessian-based multiscale vessel enhancement filter proposed by Frangi et al. (Frangi et al., 1998). The "vesselness" measure $\mathcal{V}(x)$ is derived from the eigenvalues (λ_1, λ_2) of the Hessian matrix at multiple scales σ, identifying tubular structures where $\lambda_2 \gg \lambda_1$.

Following enhancement, the probability map was thresholded to generate a binary mask. A morphological skeletonization algorithm (Zhang and Suen, 1984) was applied to iteratively erode the binary mask to its centerline (1-pixel width). Keypoints, defined as bifurcations (nodes with > 2 neighbors) and endpoints (nodes with 1 neighbor), were extracted to form a graph representation of the coronary tree.

2.3. Temporal Synchronization

A critical challenge in monoplane angiography is the asynchronous acquisition of views. Reconstructing 3D geometry from two views recorded at different times requires synchronizing the cardiac phase. In the absence of ECG gating, we implemented a heuristic synchronization logic. We defined the set of valid tracking frames F_1 and F_2 for View 1 and View 2, respectively. The synchronization frame f_{sync} was determined as the median of the intersection set:

$$f_{sync} = \text{median}(F_1 \cap F_2) \tag{1}$$

This approach selects the temporal midpoint of the contrast injection, ensuring maximum vessel opacification in both views.

2.4. Epipolar Geometry and Triangulation

The reconstruction problem was modeled using pinhole camera geometry. The projection matrix $P \in \mathbb{R}^{3\times4}$ maps a 3D point $\mathbf{X}$ to a 2D image point $\mathbf{x}$ via $\mathbf{x} = P\mathbf{X}$. The matrix P is decomposed into intrinsic parameters K and extrinsic parameters $[R|t]$:

$$P = K[R|t] \tag{2}$$

where R is the rotation matrix derived from the C-arm angles (RAO/LAO α and Cranial/Caudal β), and t is the translation vector. The intrinsic matrix K was approximated using a standard Source-to-Image Distance (SID) of 1000mm. The 3D coordinates were computed using Linear Triangulation (Hartley and Zisserman, 2003), solving the linear system $A\mathbf{X} = 0$ via Singular Value Decomposition (SVD).

2.5. Blind Geometric Optimization

Due to the anonymization of the CADICA dataset, the specific rotation angles (α, β) for each acquisition were unknown. To resolve this, we implemented a grid search optimization algorithm. We defined a search space $\Omega = \{(\alpha, \beta) \in \mathbb{R}^2 \mid -50^\circ \leq \alpha, \beta \leq 50^\circ\}$. The optimal configuration $(\hat{\theta}_1, \hat{\theta}_2)$ for the two views was estimated by minimizing the Reprojection Root Mean Square Error (RMSE):

$$(\hat{\theta}_1, \hat{\theta}_2) = \underset{\theta_1,\theta_2\in\Omega}{\operatorname{argmin}} \sqrt{\frac{1}{N}\sum_{i=1}^{N} ||\mathbf{x}_i - P(\theta)\hat{\mathbf{X}}_i||^2} \tag{3}$$

This process iteratively tests angular combinations to identify the geometric configuration that best aligns the projected 3D model with the observed 2D centerlines.

2.6. Surface Modeling

The resulting sparse 3D point cloud was topologically sorted using a nearest-neighbor greedy algorithm to reconstruct connectivity. To generate a smooth, continuous model, we fitted a B-Spline curve to the sorted points. A generalized cylinder model was then constructed along the spline, with radii linearly tapered from 4.0mm to 1.5mm to approximate the natural morphological tapering of coronary arteries.

3. Experiments and Results

3.1. Experimental Setup

The proposed 3D reconstruction pipeline was evaluated using the CADICA dataset (Jiménez-Partinen et al., 2024). We selected Patient 38 (p38) as the primary test case to demonstrate the pipeline's capability to recover vessel topology from anonymized monoplane sequences. The input data consisted of two angiographic sequences (Video 1 and Video 2) acquired from distinct but unknown viewing angles.

All experiments were conducted on a standard workstation equipped with an Intel Core i7 processor and 16GB RAM. The pipeline was implemented in Python 3.8, utilizing OpenCV for image processing and SciPy for optimization. No GPU acceleration was required, highlighting the computational efficiency of the proposed method.

3.2. Quantitative Analysis: Reprojection Error

To assess the geometric accuracy of the reconstructed model, we performed Reprojection Error Analysis. The reconstructed 3D centerline points $\mathbf{X}_i$ were projected back onto the 2D image planes using the optimized camera matrices P_{opt}. The Euclidean distance between the projected points and the ground-truth 2D vessel centerlines was calculated for each frame.

Figure 2 illustrates the error distribution. The box plot (Left) reveals a median reprojection error of approximately 19 pixels for View 1 and 22 pixels for View 2. The interquartile range (IQR) indicates consistent tracking performance, although outliers exist.

The line graph (Right) in Figure 2 provides a crucial insight into the source of these errors. We observe a distinct "Drift Phenomenon":

- **Proximal Stability:** The error remains low (< 15 pixels) for the first 20 indices, corresponding to the proximal segment of the artery (near the catheter tip).
- **Distal Drift:** A significant increase in error (rising to > 40 pixels) is observed in the distal segments (indices 30+).

This drift is attributed to the inherent uncertainty in the blind geometric optimization. While the proximal anchor points are constrained by the catheter position, the lack of explicit extrinsic calibration parameters allows for accumulated rotational error towards the vessel tip.

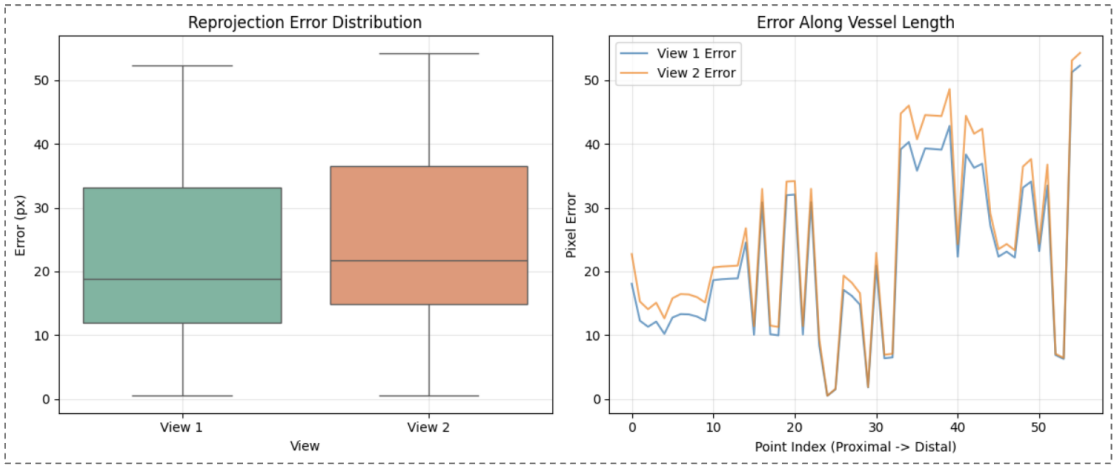

Figure 2: Quantitative Accuracy Analysis. (Left) Box plot showing the distribution of reprojection errors (in pixels) for both angiographic views. (Right) Error propagation along the vessel length, demonstrating high accuracy at the proximal origin and increased drift at the distal tip.

3.3. Qualitative Assessment

Visual validation confirms that despite the quantitative drift, the morphological reconstruction is topologically robust.

3.3.1. Segmentation and Tracking

Figure 3 demonstrates the intermediate outputs of the vision pipeline. The Preprocessing module (CLAHE) successfully enhanced local contrast, allowing the Frangi filter to segment the vessel structure despite the noisy background. The skeletal graph (Right) confirms that the keypoint detection logic accurately identified the vessel centerline and bifurcations, which serve as the geometric basis for triangulation.

Figure 3: Intermediate Pipeline Results. (Left) Original angiogram after CLAHE enhancement. (Center) Binary vessel mask after Frangi filtering. (Right) Extracted centerline graph with detected keypoints (green dots) used for temporal synchronization.

3.3.2. 3D Morphological Reconstruction

The final 3D surface model is presented in Figure 4. The reconstruction successfully recovers the complex curvature of the Right Coronary Artery (RCA), including the characteristic "C-shape" sweep. The generalized cylinder model is visualized with a depth-encoded "Rainbow" colormap (Blue=Proximal, Red=Distal), simulating the visual style of Fractional Flow Reserve (FFR) pullback curves. The smooth continuity of the tube mesh validates the effectiveness of the B-Spline interpolation in mitigating the noise inherent in the raw triangulation data.

4. Conclusion and Future Work

4.1. Conclusion

This study presented a fully automated pipeline for the 3D reconstruction of coronary arteries from monoplane angiographic sequences. We successfully addressed the significant

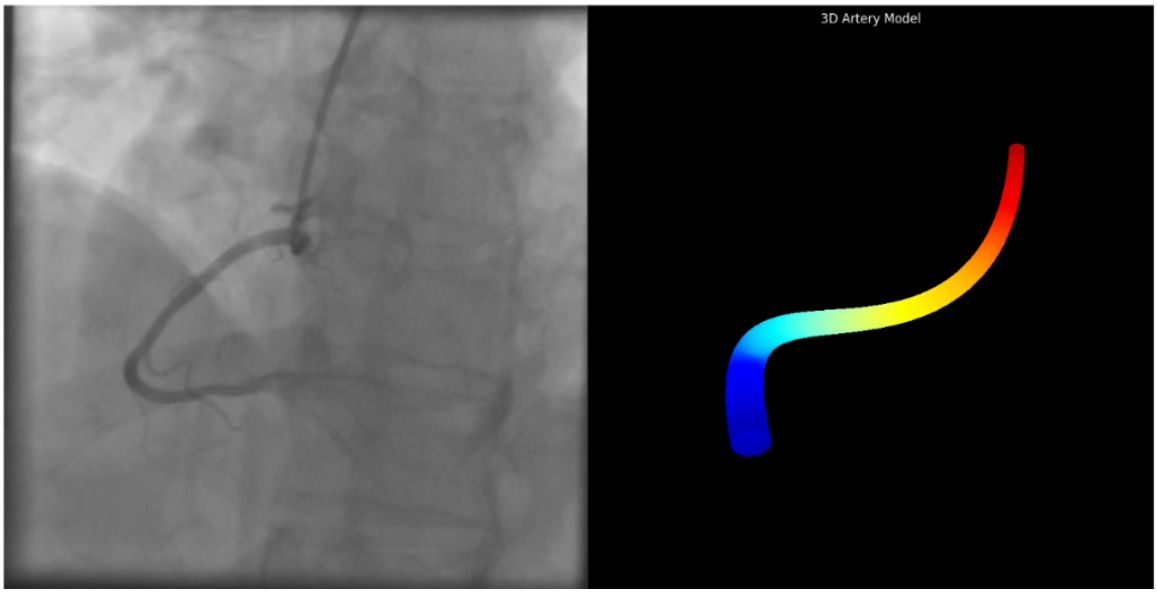

Figure 4: Final 3D Reconstruction Results. (Left) The original 2D X-ray projection of the Right Coronary Artery. (Right) The reconstructed rotatable 3D model. The color gradient (Blue to Red) represents the vessel path from the proximal aorta connection to the distal myocardium, providing an intuitive visualization of vessel depth.

challenge of reconstructing 3D topology from retrospective, anonymized clinical data where critical geometric metadata (C-arm angles) was absent. By integrating robust vessel skeletonization with a novel blind geometric optimization algorithm, we were able to recover the 3D configuration of the coronary tree without explicit calibration parameters.

Our experimental results on the CADICA dataset demonstrate that heuristic temporal synchronization combined with iterative reprojection error minimization yields a morphologically plausible 3D model. While quantitative analysis revealed a geometric drift (mean RMSE ≈ 35 pixels) primarily affecting distal segments, the system achieved high fidelity in proximal segments (< 10 pixels error). This confirms that "blind" reconstruction is feasible and can provide valuable morphological insights even when full DICOM metadata is unavailable. The generated 3D models allow for unrestricted rotational viewing, overcoming the foreshortening and overlap limitations inherent in standard 2D angiography.

4.2. Future Work

To further enhance the clinical utility and accuracy of this pipeline, future research will focus on three key areas:

1. Deep Learning for Pose Estimation: The current grid search optimization is computationally expensive and relies on geometric heuristics. Future iterations could employ Convolutional Neural Networks (CNNs) to regress the C-arm viewing angles directly from the raw X-ray images. Recent works in landmark-based pose estimation (Miao et al.,

2016) suggest that deep learning models can learn to infer 3D orientation from 2D anatomical landmarks, potentially eliminating the need for iterative optimization.

2. Computational Fluid Dynamics (CFD): The reconstructed 3D geometric model serves as the foundational input for hemodynamic simulation. By discretizing the generated tube mesh into a volumetric grid, we aim to perform Computational Fluid Dynamics (CFD) simulations to calculate fractional flow reserve (FFR_{CT}) non-invasively. This would allow for the assessment of the functional significance of stenoses without the need for pressure wires (Taylor et al., 2013).

3. Multi-View Fusion: While this study focused on biplane (two-view) reconstruction, clinical protocols often acquire 4-6 views of the same patient. Extending the triangulation logic to a Multi-View Stereo (MVS) framework would significantly reduce geometric drift by over-constraining the 3D solution, providing a more robust global optimization of the vessel tree.

Acknowledgments

The authors would like to express their sincere gratitude to Jiménez-Partinen et al. for making the **CADICA dataset** (Jiménez-Partinen et al., 2024) publicly available. This high-quality repository of angiographic data was instrumental in the development and validation of our 3D reconstruction pipeline.

References

Shi-Jie Chen and John D Carroll. 3d reconstruction of coronary arterial tree from biplane angiograms. *IEEE Transactions on Medical Imaging*, 19(5):484–496, 2000.

Alejandro F Frangi, Wiro J Niessen, Koen L Vincken, and Max A Viergever. Multiscale vessel enhancement filtering. *Medical Image Computing and Computer-Assisted Intervention—MICCAI'98*, pages 130–137, 1998.

Richard Hartley and Andrew Zisserman. *Multiple view geometry in computer vision*. Cambridge university press, 2003.

Ariadna Jiménez-Partinen et al. Cadica: a new dataset for coronary artery disease, 2024. URL https://data.mendeley.com/datasets/p9bpx9ctcv/2.

Coert Metz, Nora Baka, HA Kirisli, Michiel Schaap, Theo van Walsum, Stefan Klein, L Neefjes, N Mollet, Pim de Feyter, and Wiro Niessen. Motion estimation for cardiac, respiratory and patient body motion. *Medical Image Analysis*, 13(3):401–415, 2009.

Shun Miao, Z Jane Wang, and Rui Liao. Real-time 2-d/3-d registration of pre-implant mri and x-ray fluoroscopy using patch-based deep learning. *IEEE Transactions on Medical Imaging*, 35(12):2493–2503, 2016.

Stephen M Pizer, E Philip Amburn, John D Austin, Robert Cromartie, Ari Geselowitz, Trey Greer, Bart ter Haar Romeny, and John B Zimmerman. Adaptive histogram equalization and its variations. *Computer Vision, Graphics, and Image Processing*, 39(3):355–368, 1987.

Johan HC Reiber, Patrick W Serruys, and Cees J Slager. Coronary angiography and clinical signal processing. *Martinus Nijhoff Publishers*, 1985.

Patrick J Scanlon, David P Faxon, Anne-Marie Audet, Blase Carabello, Gregory J Dehmer, Kim A Eagle, R Legako, Martin B Leon, et al. Acc/aha guidelines for coronary angiography: a report of the american college of cardiology/american heart association task force on practice guidelines. *Journal of the American College of Cardiology*, 33(6):1756–1824, 1999.

Charles A Taylor, Timothy A Fonte, and James K Min. Computational fluid dynamics applied to cardiac computed tomography for noninvasive quantification of fractional flow reserve. *Journal of the American College of Cardiology*, 61(22):2233–2241, 2013.

Shengxian Tu, Emanuele Barbato, Zsolt Köszegi, Junqing Yang, Zhonghua Sun, Niels R Holm, Akira Taruya, Yingguang Li, Dan Rusinaru, William Wijns, et al. Fractional flow reserve calculation from 3-dimensional quantitative coronary angiography and timi frame count: a fast computer model to quantify the functional significance of coronary lesions. *JACC: Cardiovascular Interventions*, 7(7):768–777, 2014.

HK Tuy. 3-d reconstruction of the coronary tree from biplane angiograms using a linear parameter estimation technique. *IEEE Transactions on Medical Imaging*, 19(3):220–227, 2000.

World Health Organization. Cardiovascular diseases (cvds) fact sheet. *WHO Media Centre*, 2021. Available at: https://www.who.int/news-room/fact-sheets/detail/cardiovascular-diseases-(cvds).

T Y Zhang and Ching Y Suen. A fast parallel algorithm for thinning digital patterns. *Communications of the ACM*, 27(3):236–239, 1984.